Finite–Element Analyses of Combined Void Shape and Plastic Anisotropy Effects in Ductile Fracture

A. A. Benzerga and S. M. Keralavarma

Department of Aerospace Engineering, Texas A&M University,

College Station, TX 77843, USA

Abstract

Prediction of ductile fracture in structural metallic materials requires some representation of microstructural effects, including the plastic anisotropy that is associated with initial or induced polycrystalline textures and the microscopic processes of void growth and coalescence. With the objective of characterizing existing continuum models, we present a finite-element study of cylindrical unit cells, consisting of spheroidal voids embedded in an orthotropic Hill matrix, subjected to proportional loading paths. Two-dimensional axisymmetric calculations are employed for the case of transverse isotropy and axisymmetric loading about the void axis. The effective cell model responses are compared with predictions from an extended model of anisotropic void growth, which is the subject of an accompanying paper.

1 Introduction

This paper is concerned with damage-induced cracking that potentially occurs when large plastic deformations are involved, such as in metal forming operations. In structural materials, ductile fracture initiates at second-phase particles due to the nucleation of voids, which subsequently grow to coalescence [1]. The material then goes from a state of diffuse damage to a state where, for the first time, one or more macroscopic cracks have initiated. Fig. 1 illustrates the key physical processes involved. Void growth is tightly connected to matrix plasticity and is weakly dependent upon the spatial distribution of voids. The latter is a direct consequence of the distribution of particles from which the voids initiate in the first place. However, void coalescence is a collective phenomenon and is strongly affected by void distribution [3]. These basic mechanisms of ductile fracture are now well established [1].

From the elementary micromechanisms described in Fig. 1 it appears that, physically, void growth and coalescence are but an expression of certain modes of

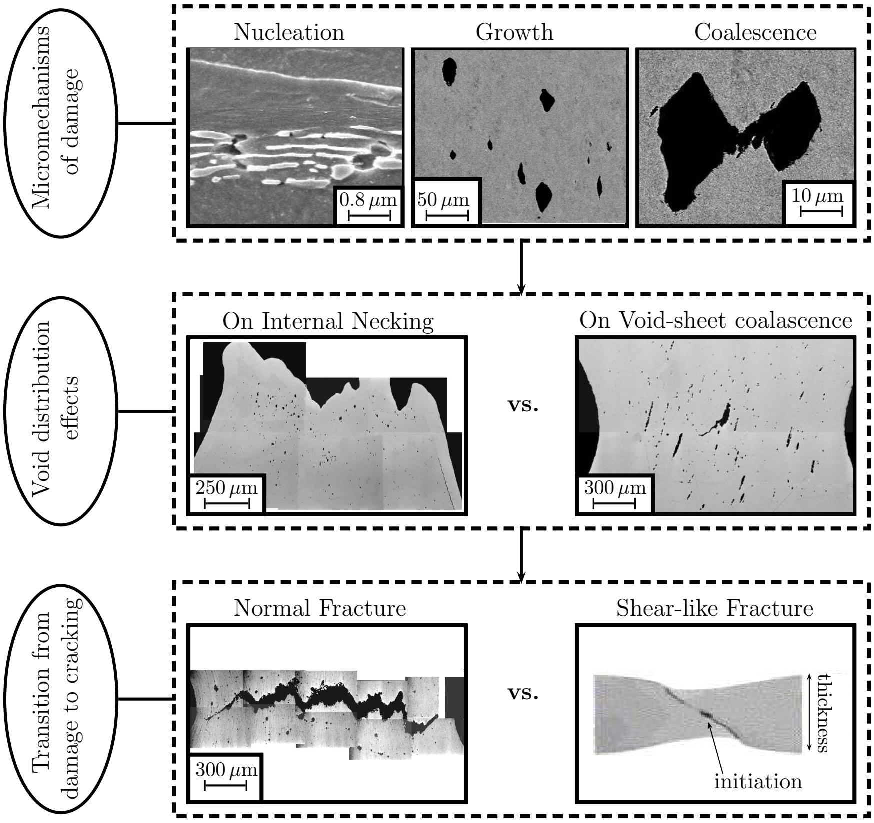

Figure 1: Top: Elementary microscopic mechanisms of ductile damage. Middle: Effects of void distribution and void rotation on coalescence; Bottom: Normal "zigzag" vs. shear-like fracture. All but bottom right micrograph are adapted from [2].

plastic deformation of the surrounding material. Because the generic micromechanisms of ductile damage are well known, the phenomenon naturally lends itself to be treated by means of homogenization theory. The ideal framework for modeling ductile fracture is one that has a good representation of plastic deformation, e.g. polycrystalline model for metals and alloys, combined with the ability to predict void nucleation, growth and coalescence. The homogenization problem is unfortunately not tractable analytically with too sophisticated a plasticity model for the matrix. In fact, this has led to the famous Gurson model [4] and subsequent generalizations [5, 6]. The Gurson micromechanics is based on the Von Mises plasticity model with no hardening. It has provided a foundation for an attractive computational methodology for modeling and simulation of ductile fracture [7, 8]. However, under the large plastic deformations that precede fracture, the basic representative volume element itself evolves. This microstructural evolution leads to induced anisotropy. To account for this, extensions of the Gurson model were developed in recent years to incorporate void shape effects [5, 9] and plastic anisotropy of the matrix material [6]. In addition, micromechanical unit-cell calculations [3, 10, 11] have also documented the effect of void shape and distribution on void coalescence. This has motivated the development of improved coalescence models [10, 12–14].

Based on the above extensions of the Gurson model, Benzerga and co-workers [2, 15, 16] introduced a new ductile fracture computational methodology, which accounts for certain types of initial and induced anisotropy. The fundamental hypothesis of their approach is that the microstructure, defined at an appropriate scale, and its evolution play a major role in determining ductile damage accumulation. This hypothesis has already been tested with some success in the context of high strength steels [15, 16]. Their approach, however, was based on a heuristic combination of void shape and plastic anisotropy effects. In this paper, we show the limits of such heuristics and investigate the coupling between void shape and plastic anisotropy effects by means of direct finite element cell calculations of the type pioneered by Koplik and Needleman [3]; also see [6, 10, 11]. By the same account, we demonstrate the need for improved models of ductile fracture and advocate one such model that was recently developed by the authors [17, 18].

2 Voided Cell Calculations

2.1 Principle and Setup

Assume a periodic or regular distribution of spheroidal voids sharing a common axis. This entails no loss of generality since void growth is insensitive to the spatial distribution of cavities [3, 13]. Hence, the calculations are based on the concept of a unit-cell containing a single void (Fig. 2) as elaborated upon in [8]. The initial void volume fraction, f_0, is fixed to 0.001 while the initial void aspect ratio, w_0, is varied between 1/2 and 2. The matrix is taken to be elasto-plastic with

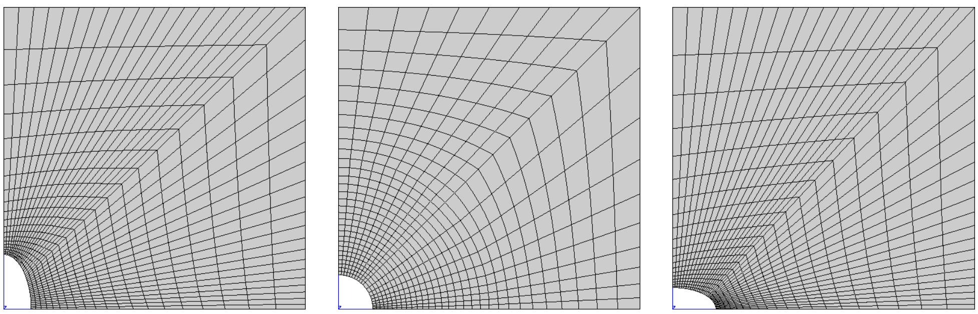

(a) (b) (c)

Figure 2: Finite element meshes used in the axisymmetric calculations (a) prolate void ($w_0 = 2$); (b) spherical void ($w_0 = 1$); and (c) oblate void ($w_0 = 1/2$). Initial porosity is $f_0 = 0.001$ in all three cases.

elastic constants $E = 210$ GPa and $\nu = 0.3$. The plasticity model is defined by a quadratic Hill criterion with associated flow rule and power-law hardening (with exponent 0.1). Invariance of material flow properties about an axis is assumed. In that case, the yield criterion is completely defined by three independent Hill coefficients and the elastic limit in a given direction, say σ_1. Three materials are investigated, Table 1. Axisymmetric loadings are considered with a major axial

Name	h_1	h_2	h_3	h_4	h_5	h_6
Isotropic	1.000	1.000	1.000	1.000	1.000	1.000
Material (i)	1.000	1.000	1.000	3.667	3.667	1.000
Material (iii)	1.000	1.000	1.000	0.500	0.500	1.000

Table 1: Material anisotropy parameters used in the computations.

stress. Therefore, there are three different axes of symmetry associated with the void, the material and the loading. Attention is restricted to the simplest, yet most practical, case where all three axes are aligned so that axisymmetric calculations can be used.

The object-oriented finite element (FE) code ZeBuLoN [19] is employed using a Lagrangian formulation of the field equations. Fig. 2 shows the FE meshes used, which consist of sub-integrated quadratic quadrilateral elements. Special boundary conditions are formulated such that the ratio θ of net axial stress, Σ_{zz}, to net lateral stress, Σ_{rr}, remains constant throughout the calculation. Stress triaxiality is measured by the ratio $\mathcal{T}$ of the mean normal stress, Σ_m, to the equivalent stress Σ_e, given by:

$$\Sigma_e = |\Sigma_{zz} - \Sigma_{rr}|, \quad \Sigma_m = \frac{1}{3}(\Sigma_{zz} + 2\Sigma_{rr}), \quad \mathcal{T} = \frac{\Sigma_m}{\Sigma_e} = \frac{1}{3}\frac{2\theta + 1}{|1-\theta|} \qquad (1)$$

A macroscopic effective strain, E_e, is defined work-conjugate with Σ_e. A Riks algorithm [20] is used to integrate the nonlinear constitutive equations in order to keep the stress ratio θ, and hence $\mathcal{T}$, constant. Here $\mathcal{T} = 1$ in all calculations.

2.2 Results

First, consider the case of spheroidal voids embedded in an isotropic matrix. The corresponding effective stress versus strain responses are compared in Fig. 3 with that of an initially isotropic solid ($w_0 = 1$ and isotropic matrix). Each response depicts the basic phenomenology of void growth to coalescence. In a typical calculation, the stress drop coincides with the onset of void coalescence, which is accompanied by accelerated lateral void growth. The results in Fig. 3 demonstrate the effect of initial void shape on void growth rates, in keeping with previous studies [10].

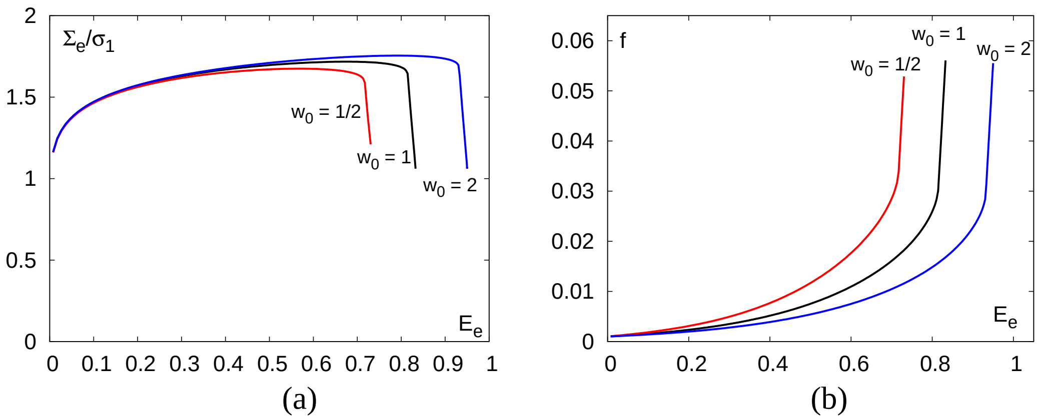

Figure 3: Effect of initial void aspect ratio, w_0, on (a) effective stress–strain response; and (b) evolution of porosity, for an isotropic matrix.

Next, consider the case of spherical voids in a Hill matrix. All material parameters are kept fixed except the Hill anisotropy factors that characterize plastic flow of the matrix material. This is the case treated by Benzerga and Besson [6] except that the results here include the stage of void coalescence. The results in Fig. 4 clearly show the drastic effect of plastic anisotropy on the overall response of the unit cell. The macroscopic effective stress, Σ_e is normalized by σ_1, the initial yield stress of the matrix along the z-axis. Although neglected in nearly all ductile fracture analyses, the effect of plastic anisotropy on void growth rate is more substantial than that of void shape considering realistic ranges for the material parameters. This result is not surprising: as noted in the introduction, void growth is merely

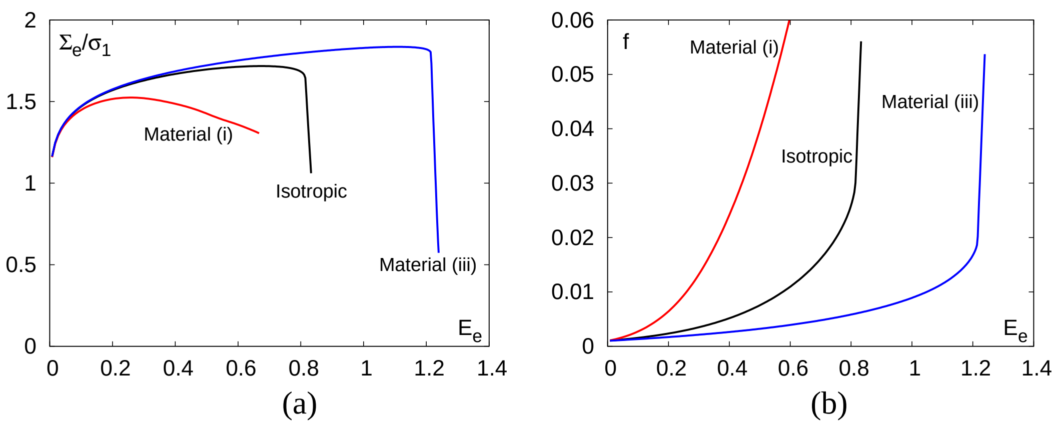

Figure 4: Effect of material anisotropy on (a) stress–strain response; and (b) evolution of porosity, for an initially spherical void.

the expression of plastic deformation of the matrix; there is no internal pressure within the voids. Therefore, it is naturally expected that the ease, or difficulty, with which plastic flow occurs in the matrix will affect the void growth process. The results in Fig. 4 provide a quantification of such an expected effect.

Finally, consider the combined effect of plastic anisotropy and void shape, i.e., spheroidal voids embedded in a Hill matrix. The result can be totally unexpected, as illustrated in Fig. 5. In material (i) (representative of aluminum alloys) the effect of void shape is retained, though less than in the isotropic case; compare to Fig. 3. However, in material (iii) (which is representative of a zirconium alloy), the effect of void shape essentially disappears, at least within the range of w_0 considered here. The first conclusion is that the combined effect is not a simple superposition of separate effects, as tacitly assumed earlier by Benzerga et al. [16]. Perhaps, the most important conclusion from Fig. 5 is that the first-order effect that clearly remains is that of plastic anisotropy: when the porosity has reached ten times its initial value (i.e. when $f = 0.01$) the difference in effective strain between the two materials, averaged over the set of values for w_0 considered here, is greater than 0.8; compare to a difference of ≈ 0.2 induced by changes in w_0 in the case of an isotropic matrix.

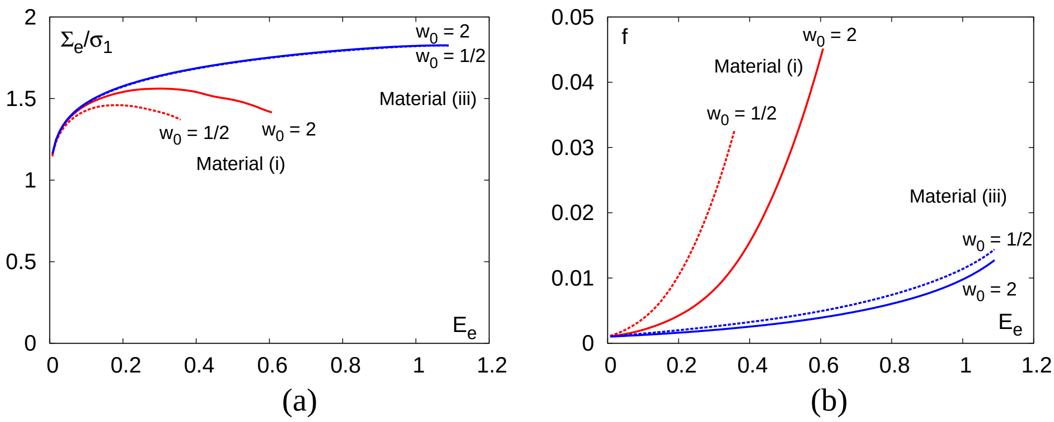

Figure 5: Combined effect of material anisotropy and void shape on (a) stress–strain response; and (b) evolution of porosity, for two different anisotropic matrices.

In examining the way in which plastic flow develops in the matrix, the effect of plastic anisotropy is found to be even more subtle than discussed above. Fig. 6 shows contours of effective plastic strain at the same macroscopic effective strain $E_e = 0.45$. The contours correspond to the calculations shown in Fig. 4. It can be seen that the void in material (i) develops into a peculiar shape caused by the formation of a shear band with intense plastic deformation. Recall that the calculation is axisymmetric, which means that a cone of localized deformation has formed. This type of behavior is usually precluded under axisymmetric loadings [21] but seems to be promoted by plastic flow anisotropy of some specific kind. In this connection, two observations are worth making. On average the initially spherical void elongates more rapidly in material (i) (Fig. 6(a)); yet that is the material with lowest ductility (Fig. 4). This is in contrast with existing void growth models [2, 5, 10], which would predict greater ductility in a material with most elongated voids. Moreover, while void-coalescence occurs through localization of plastic deformation in a ligament perpendicular to the major traction (so-called internal necking mode) in material (iii) and the isotropic material (Figs. 6(b) and (c)), the behavior is totally different in material (i) where void-coalescence tends to occur along an inclined band.

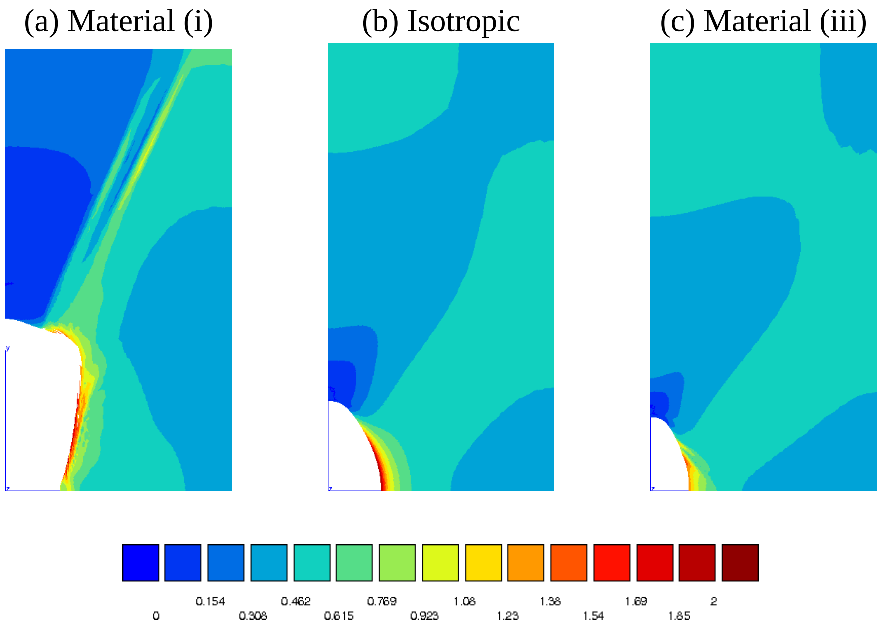

Figure 6: Contours of effective plastic strain in deformed configurations at $E_e = 0.45$ for (a) Material (i); (b) isotropic matrix; and (c) Material (iii). Void is initially spherical in all.

3 Extended Void Growth Model

3.1 Synopsis

In a companion paper [18], a micromechanics-based model of void growth in anisotropic materials is developed. Below is a streamlined presentation of the resulting constitutive equations. The effective yield criterion is derived as [18]:

$$C\frac{3}{2}\frac{\mathbf{\Sigma} : \mathbb{H} : \mathbf{\Sigma}}{\sigma_m^2} + 2q(g+1)(g+f)\cosh\left(\kappa\frac{\mathbf{\Sigma} : \mathbf{X}}{\sigma_m}\right) - (g+1)^2 - q^2(g+f)^2 = 0 \quad (2)$$

Here, $\mathbb{H}$ is an effective anisotropy tensor defined by

$$\mathbb{H} \equiv (\mathbb{J} + \eta\mathbf{X}\otimes\mathbf{Q}) : \mathbb{h} : (\mathbb{J} + \eta\mathbf{Q}\otimes\mathbf{X}) \quad (3)$$

where $\mathbb{h}$ is Hill's orthotropy tensor for the matrix in deviatoric-stress space [6] and $\mathbb{J}$ is the deviatoric projection tensor defined by $\mathbb{J} \equiv \mathbb{1} - \frac{1}{3}\mathbf{1}\otimes\mathbf{1}$ where $\mathbb{1}$ and

$\mathbf{1}$ are the fourth- and second-order identity tensors, respectively. Also, $\mathbf{X}$ and $\mathbf{Q}$ are second-order tensors tied to the current void orientation by

$$\mathbf{X} \equiv \alpha_2(\mathbf{e}_1 \otimes \mathbf{e}_1 + \mathbf{e}_2 \otimes \mathbf{e}_2) + (1 - 2\alpha_2)\mathbf{e}_3 \otimes \mathbf{e}_3 \tag{4}$$

$$\mathbf{Q} \equiv -\frac{1}{2}(\mathbf{e}_1 \otimes \mathbf{e}_1 + \mathbf{e}_2 \otimes \mathbf{e}_2) + \mathbf{e}_3 \otimes \mathbf{e}_3 \tag{5}$$

where $(\mathbf{e}_1, \mathbf{e}_2, \mathbf{e}_3)$ is an orthonormal Cartesian frame with $\mathbf{e}_3$ aligned with the void axis and $\mathbf{e}_1, \mathbf{e}_2$ chosen arbitrarily. Finally, C, η, κ, g and α_2 are scalar-valued functions of the microstructural variables, namely the porosity, f, the void aspect ratio, w, and three scalar anisotropy factors, h, h_t and h_a, which are linear functions of the components of $\mathbb{h}$. The functional forms of all the scalar parameters in the model are provided in [18].

Criterion (2) is supplemented with an associated flow rule and a heuristic extension to hardening. With σ_m the matrix yield stress in a reference direction, denote the matrix effective plastic strain by $\bar{\epsilon}^p_m$; then the evolution of $\bar{\epsilon}^p_m$ is given by [4]

$$(1 - f)\sigma_m \dot{\bar{\epsilon}}^p_m = \mathbf{\Sigma} : \mathbf{D}^p \tag{6}$$

where $\mathbf{D}^p$ is the plastic deformation rate. The heuristic parameter, q, is taken to be a function of the current void aspect ratio following [5].

$$q = 1 + (q_s - 1)\frac{2w}{1 + w^2} \tag{7}$$

where q_s is the value of q for a spherical void, taken to be equal to 1.6 in the computations presented here.
The evolution equations for the microstructural variables, f and w, are given by

$$\dot{f} = (1 - f)\,\mathrm{tr}(\mathbf{D}^p), \qquad \dot{w} = \frac{1}{2}(2D^v_{33} - D^v_{11} - D^v_{22})w \tag{8}$$

where $\mathbf{D}^v$ is the average deformation rate of the void. The latter is determined as a function of the macroscopic plastic deformation rate, $\mathbf{D}^p$, using the relationship developed by Ponte Castaneda and Zaidman [22]:

$$\mathbf{D}^v = \mathbb{A} : \mathbf{D}^p, \qquad \mathbb{A} \equiv [\mathbb{1} - (1 - f)\mathbb{S}]^{-1} \tag{9}$$

where $\mathbb{A}$ is a ‘concentration’ tensor for the deformation rate and $\mathbb{S}$ is the Eshelby tensor for a spheroidal void in an infinite linear-viscous isotropic matrix [23]. An equation for the spin rate is also derived in [18] but is not relevant here.

3.2 Toward Validation

The above constitutive equations are integrated for imposed stress paths that mimic those used in the unit-cell calculations. Integration is carried out using a backward Euler scheme. Fig. 7 shows a comparison between model and FE calculations. The correspondence is very good given that the only heuristic adjustment resides in the q parameter, which does not depend on plastic anisotropy.

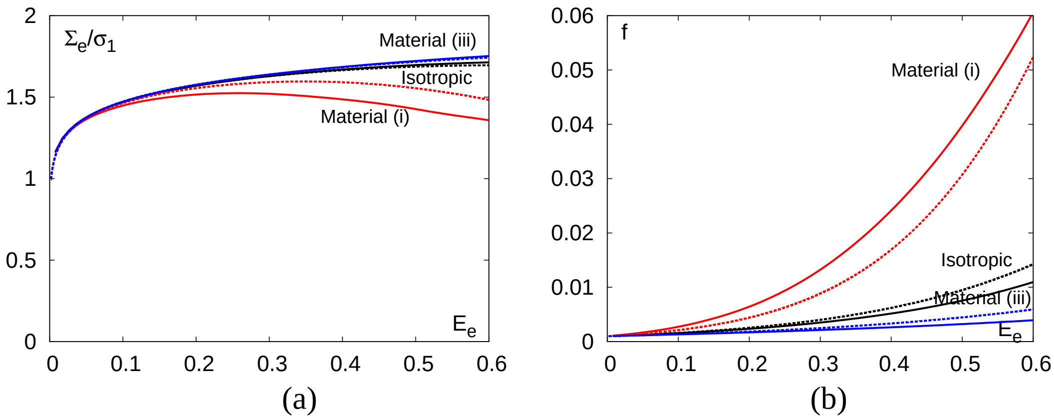

Figure 7: Comparison of unit-cell responses (solid curves) and model predictions (dashed curves) in the pre-coalescence regime for (a) the stress–strain response; and (b) the evolution of porosity, for $w_0 = 1$ and three matrix materials.

4 Closure

Micromechanical finite-element calculations have been carried out to investigate the coupling between micro-scale plastic anisotropy and void growth. State-of-the-art models of void growth fail to capture the basic coupling. Comparison of the FE calculations with an extended model of void growth, recently developed by the authors, shows promising results both in terms of effective response and microstructure evolution.

References

[1] A. Pineau, T. Pardoen, Failure of Metals, Comprehensive Structural Integrity 2 (2007) 684–797, Chapter 2.06.

[2] A. A. Benzerga, Ph.D. thesis, Ecole des Mines de Paris (2000).

[3] J. Koplik, A. Needleman, Void growth and coalescence in porous plastic solids, Int. J. Solids Structures 24 (8) (1988) 835–853.

[4] A. L. Gurson, Continuum Theory of Ductile Rupture by Void Nucleation and Growth: Part I– Yield Criteria and Flow Rules for Porous Ductile Media, J. Eng. Mat. Tech. 99 (1977) 2–15.

[5] M. Gologanu, J.-B. Leblond, G. Perrin, J. Devaux, Recent extensions of Gurson's model for porous ductile metals, in: P. Suquet (Ed.), CISM Lectures Series, Springer, New York, 1997, pp. 61–130.

[6] A. A. Benzerga, J. Besson, Plastic potentials for anisotropic porous solids, Eur. J. Mech. 20 (3) (2001) 397–434.

[7] V. Tvergaard, A. Needleman, Analysis of the cup–cone fracture in a round tensile bar, Acta metall. 32 (1984) 157–169.

[8] V. Tvergaard, Material failure by void growth to coalescence, Advances in Applied Mechanics 27 (1990) 83–151.

[9] M. Garajeu, J. C. Michel, P. Suquet, A micromechanical approach of damage in viscoplastic materials by evolution in size, shape and distribution of voids, Comput. Methods Appl. Mech. Engrg 183 (2000) 223–246.

[10] T. Pardoen, J. W. Hutchinson, An extended model for void growth and coalescence, J. Mech. Phys. Solids 48 (2000) 2467–2512.

[11] X. Gao, T. Wang, J. Kim, On ductile fracture initiation toughness: Effects of void volume fraction, void shape and void distribution, Int. J. Solids Structures 42 (2005) 5097–5117.

[12] M. Gologanu, J.-B. Leblond, G. Perrin, J. Devaux, Theoretical models for void coalescence in porous ductile solids – I: Coalescence in "layers", Int. J. Solids Structures 38 (2001) 5581–5594.

[13] A. A. Benzerga, Micromechanics of Coalescence in Ductile Fracture, J. Mech. Phys. Solids 50 (2002) 1331–1362.

[14] J.-B. Leblond, G. Mottet, A theoretical approach of strain localization within thin planar bands in porous ductile materials, C. R. Mecanique 336 (2008) 176–189.

[15] A. A. Benzerga, J. Besson, R. Batisse, A. Pineau, Synergistic effects of plastic anisotropy and void coalescence on fracture mode in plane strain, Modelling Simul. Mater. Sci. Eng. 10 (2002) 73–102.

[16] A. A. Benzerga, J. Besson, A. Pineau, Anisotropic ductile fracture. Part II: theory, Acta Mater. 52 (2004) 4639–4650.

[17] S. M. Keralavarma, A. A. Benzerga, An approximate yield criterion for anisotropic porous media, C. R. Mecanique 336 (2008) 685–692.

[18] S. M. Keralavarma, A. A. Benzerga, A micromechanics-based ductile damage model incorporating plastic anisotropy and void shape effects, in: $12^{\rm th}$ International Conference on Fracture, 2009, pp. CD–ROM.

[19] J. Besson, R. Foerch, Large scale object oriented finite element code design, Comput. Methods Appl. Mech. Engrg 142 (1997) 165–187.

[20] E. Riks, An incremental approach to the solution of snapping and buckling problems, Int. J. Solids Structures 15 (1979) 529–551.

[21] J. Rice, The localization of plastic deformation, in: W. Koiter (Ed.), North–Holland, Amsterdam, 1976, pp. 207–220.

[22] P. Ponte Castañeda, M. Zaidman, Constitutive models for porous materials with evolving microstructure, J. Mech. Phys. Solids 42 (1994) 1459–1495.

[23] J. Eshelby, The determination of the elastic field of an ellipsoidal inclusion, and related problems, Proc. Roy. Soc A241 (1957) 357–396.